

## Proton-capture reactions in thermonuclear supernovae and the $p$ process

---

**Kerstin Sonnabend\***, **C. Arda**, **A. Endres**, **P. Erbacher**, **J. Glorius**, **K. Göbel**, **O. Hinrichs**, **M. Reich**, **B. Thomas**, and **T. Thomas** <sup>†</sup>

*Institut für Angewandte Physik, Goethe Universität Frankfurt, Germany*

*E-mail:* [sonnabend@iap.uni-frankfurt.de](mailto:sonnabend@iap.uni-frankfurt.de)

As an alternative production scenario to the so-called  $\gamma$  process, the most abundant  $p$  nucleus  $^{92}\text{Mo}$  may be produced by a chain of proton-capture reactions in supernovae type Ia. The reactions  $^{90}\text{Zr}(p,\gamma)$  and  $^{91}\text{Nb}(p,\gamma)$  are the most important reactions in this chain. We have measured the first reaction using high-resolution in-beam  $\gamma$ -spectroscopy at HORUS, Cologne, Germany, to contribute to the existing experimental data base. So far, we only investigated the high-energy part of the Gamow window and the analysis is still in progress. We plan to study the second reaction in standard kinematics at the FRANZ facility, Frankfurt, Germany. Current developments at FRANZ will be explained in detail.

*XIII Nuclei in the Cosmos,  
7-11 July, 2014  
Debrecen, Hungary*

---

\*Speaker.

<sup>†</sup>We thank the group of A. Zilges and the accelerator staff at University of Cologne, Germany, for their enormous support during the beam time. This work is supported by Deutsche Forschungsgemeinschaft (SO907/2-1) and by HIC for FAIR within the framework of LOEWE launched by the State of Hesse, Germany.

## 1. Motivation

Almost all elemental abundances beyond the so-called iron peak are produced by neutron-capture reactions in the  $r$  and  $s$  processes [1]. Only about 35 isotopes on the proton-rich side of the valley of stability are bypassed by the reaction paths, thus, their existence remains to be explained by additional mechanisms of nucleosynthesis [2]. Different approaches and varying astrophysical sites of their realization are discussed, *e.g.*, the  $\gamma$  process [3], the  $rp$  process [4], the  $pn$  process [5], the  $\nu p$  process [6], and the  $\nu$  process [7] with the different names focussing on a special characteristic of the production scenario. In general, all these mechanisms can be summarized as the  $p$  process to indicate that they are involved in the synthesis of the  $p$  nuclei.

The isotope  $^{92}\text{Mo}$  is the most abundant  $p$  nucleus with an isotopic abundance of  $I_{\%} = 14.84\%$ . It has one of the smallest overproduction factors in the  $\gamma$  process [2]. A chain of radiative proton-capture reactions on the stable neutron-magic  $N = 50$  nuclei might be an additional production mechanism as proposed in [8, 9] for type Ia supernovae. Due to the increasing Coulomb barrier, the proton-capture cross sections of  $^{90}\text{Zr}$  and  $^{91}\text{Nb}$  decrease compared to the other neutron-magic isotopes with  $N = 50$ . Thus, the corresponding reaction rates determine how much  $^{92}\text{Mo}$  can stem from the explosive scenario of a type Ia supernova.

As an unstable isotope,  $^{91}\text{Nb}$  is not available in the seed distribution. Thus, every  $^{91}\text{Nb}$  nucleus has to be produced before it can capture a proton to become  $^{92}\text{Mo}$ . Therefore, the cross sections of the  $^{90}\text{Zr}(p,\gamma)$  and  $^{91}\text{Nb}(p,\gamma)$  reactions are the most important ones to understand the abundance of  $^{92}\text{Mo}$  made in this scenario. Besides the production of  $^{92}\text{Mo}$  via radiative proton-capture reactions, its destruction by the same reaction type has to be taken into account, too. However, the freshly synthesized  $^{92}\text{Mo}$  will not be destroyed directly because of the low rate of the  $^{92}\text{Mo}(p,\gamma)$  reaction which was recently experimentally confirmed by [10].

In case the reactions leading to the production of  $^{92}\text{Mo}$  are strongly influenced by the astrophysical environment, its observed abundance can be used as a benchmark test for the astrophysical conditions realized in different scenarios and nucleosynthesis network calculations. Then, it can be used as a tracer and provides an interesting look to the inside of, *e.g.*, a type Ia supernova.

## 2. Investigation of the $^{90}\text{Zr}(p,\gamma)$ reaction

Recently, a measurement by A. Spyrou and co-workers investigated the  $^{90}\text{Zr}(p,\gamma)$  reaction using the  $4\pi$  summing technique [11] to remove the systematic uncertainty introduced by two previous measurements [12, 13]. The  $4\pi$  summing technique yields the cross section independent of the level scheme of the product nucleus and is therefore comparable to the thick target yield method used by [12]. Thus, the agreement of the two measurements as stated in [11] was not surprising. To exclude an influence of the level scheme, especially of an isomeric state in  $^{91}\text{Nb}$  ( $E_{\gamma} = 104$  keV,  $t_{1/2} = 60.86$  d), we investigated the reaction using the same technique as in [13]: high-resolution in-beam  $\gamma$ -spectroscopy.

We used HORUS at University of Cologne, Germany, with a target chamber optimized for measurements of radiative particle-induced reactions in the astrophysically relevant energy range [14]. Thirteen high-purity Germanium (HPGe) detectors are placed at five different angles with respect to the incoming beam to determine the angular dependency of the prompt  $\gamma$  rays in order

to extract the total cross section. The observation of the depopulation of the so-called entry-state (marked with  $\gamma_i$  in Fig. 1) yields the partial cross sections  $(p, \gamma_i)$  [15]. Their sum equals the total cross section. However, the experimental determination of all corresponding transitions is usually hampered by a lack of knowledge of the complete level scheme up to the energy of the entry-state.

Therefore, the total cross section is usually determined from the transitions of excited levels to the ground state (marked in red in Fig. 1) which collect the contributions of all possible cascades from the entry state. Since there is an isomeric state in  $^{91}\text{Nb}$  which serves also as an end point of cascades (transitions marked in yellow in Fig. 1) the contributions to the ground state and the isomeric state must be added in this special case to derive the total cross section.

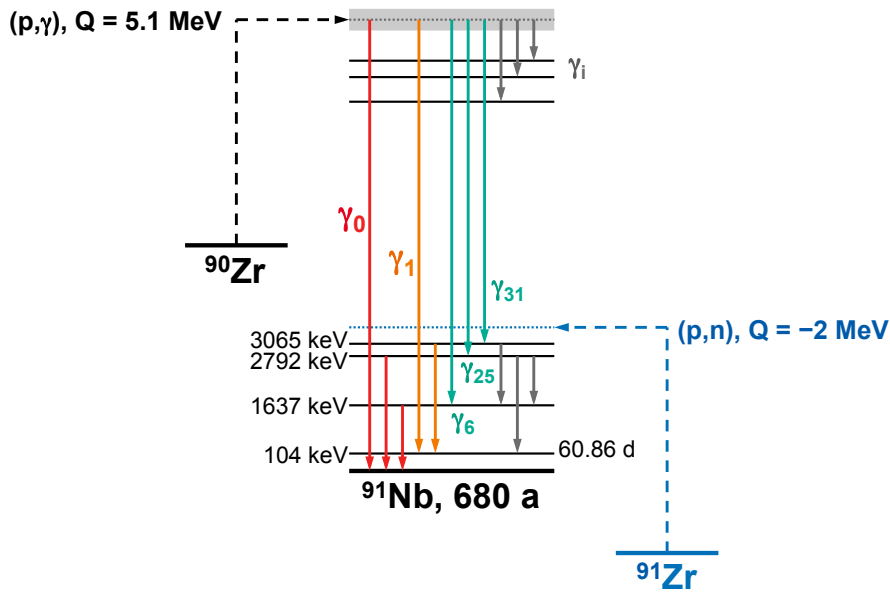


**Figure 1:** Scheme of prompt  $\gamma$  transitions of the  $^{90}\text{Zr}(p, \gamma)$  reaction (not all levels shown). The  $\gamma$  transitions depopulating the entry state (grey band) are marked with  $\gamma_i$  and correspond to the partial cross sections  $(p, \gamma_i)$ . In order to determine the total cross section, all  $\gamma$  transitions ending in the ground state (red) and the isomeric state (yellow) are analyzed and their contributions are added. Contributions stemming from the  $^{91}\text{Zr}(p, n)$  reaction populating low-energy excited states in  $^{91}\text{Nb}$  further complicate the analysis. Data from [16].

For the targets, we used isotopically enriched material consisting of 97.65%  $^{90}\text{Zr}$  and, besides other Zirconium isotopes, 0.96%  $^{91}\text{Zr}$ . As indicated in Fig. 1, the  $^{91}\text{Zr}(p, n)$  reaction feeds the same  $\gamma$  transitions as the  $^{90}\text{Zr}(p, \gamma)$  reaction to be investigated up to a certain energy. Therefore, we also prepared targets consisting of 89.20%  $^{91}\text{Zr}$  and 5.99%  $^{90}\text{Zr}$  and performed measurements with both targets for each energy. This will allow us to disentangle the contribution of both reactions from the observed reaction yields and, thus, determine the total cross sections separately. The targets had only thicknesses of  $530 \mu\text{g}/\text{cm}^2$  and were prepared as self-supporting foils in the target laboratory at Cologne. A gold foil was used to completely stop the impinging protons at the target position. The corresponding contributions in the spectra were determined using additional measurements with the gold foils only [17].

The analysis of data measured at proton energies between  $E_p = 3.6 \text{ MeV}$  and  $5.1 \text{ MeV}$  is very

time-consuming and no results on cross sections can be presented yet. To underline this statement, Fig. 2 shows a spectrum measured with a HPGe detector positioned at  $90^\circ$  with respect to the beam axis. The transitions corresponding to the depopulation of the entry-state are marked similar as in Fig. 1. In addition, a selection of the transitions needed for the determination of the total cross section are marked in red and orange, respectively.

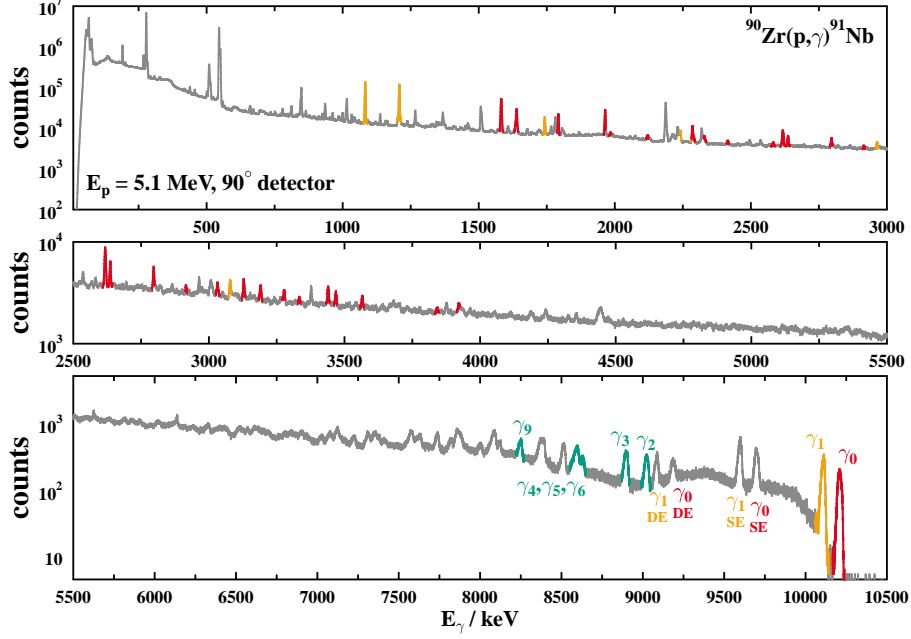


**Figure 2:** Single spectrum of a HPGe detector placed at  $90^\circ$  with respect to the beam axis in HORUS. The  $\gamma$  transitions marked in red and yellow correspond to transitions to the ground state and isomeric state of  $^{91}\text{Nb}$ , respectively, and determine the total cross section. The  $\gamma$  transitions labeled  $\gamma_i$  corresponds to the depopulation of the entry state in  $^{91}\text{Nb}$  and determine the partial cross sections (compare Fig. 1).

### 3. Towards a measurement in standard kinematics of the $^{91}\text{Nb}(p,\gamma)$ reaction

If the  $p$  nucleus  $^{92}\text{Mo}$  is produced by a series of radiative proton-capture reactions, the last one occurs on the unstable, neutron-magic isotope  $^{91}\text{Nb}$ . Usually, such a reaction will be investigated in inverse kinematics using a radioactive ion-beam facility and a gas target. Different methods are available as explained with focus on the synthesis of the  $p$  nuclei in the contributions of J. Fallis, J. Glorius, and A. Spyrou of this volume. However, the half-life of  $^{91}\text{Nb}$  is rather long with  $t_{1/2} = 680 \text{ a}$  and, thus, it is possible to investigate the  $^{91}\text{Nb}(p,\gamma)$  reaction also in standard kinematics.

Several points related to target production, beam intensity, and detection systems have to be taken into account to perform such an experiment.

1. A sufficient amount of the radioactive isotopes must be produced and prepared in a way to use it as target material.
2. The intensity of the proton beam must be high enough to provide a measurable reaction rate with the small amount of target material.

3. The target design must be suited to withstand the high power depositions caused by the high-intensity proton-beam.
4. The detection system must provide high efficiency in combination with short dead times to yield an analyzable signal-to-background ratio (see [18]).

Point 1. is addressed in detail by the contribution of B. Thomas of this volume. Taking into account the proton-beam intensity and detection system available at FRANZ, an amount of  $10^{16}$  nuclei should be sufficient to perform the experiment. In case of  $^{91}\text{Nb}$ , this translates to a total target mass in the  $\mu\text{g}$  range and an activity of the target in the MBq range.

A high-intensity proton-beam in a suitable energy range of 1.8 MeV to 2.2 MeV will be provided by the FRANZ facility, Frankfurt, Germany. The purpose of FRANZ is the production of the world's most intense neutron beams in the keV-energy range by impinging the proton beam on a  $^7\text{Li}$  target [18]. However, the proton beam is also available for studying proton-induced reactions.

The current layout of the FRANZ facility is shown schematically in Fig. 3. The protons are produced in a volume-type ion-source ( $I_p = 200$  mA,  $E_p = 120$  keV). The Low-Energy Beam-Transport (LEBT) section prepares the beam to characteristics accepted by the Radio-Frequency Quadrupole (RFQ) and the following interdigital H-mode (IH) drift tube linac. Afterwards, the beam has an energy of  $2\text{ MeV} \pm 1\%$  due to the high space-charge density. The design current is up to 20 mA in a quasi-continuous wave mode as the time structure of the RFQ and IH with a repetition rate of 175 MHz and bunch lengths of 1 ns persists.

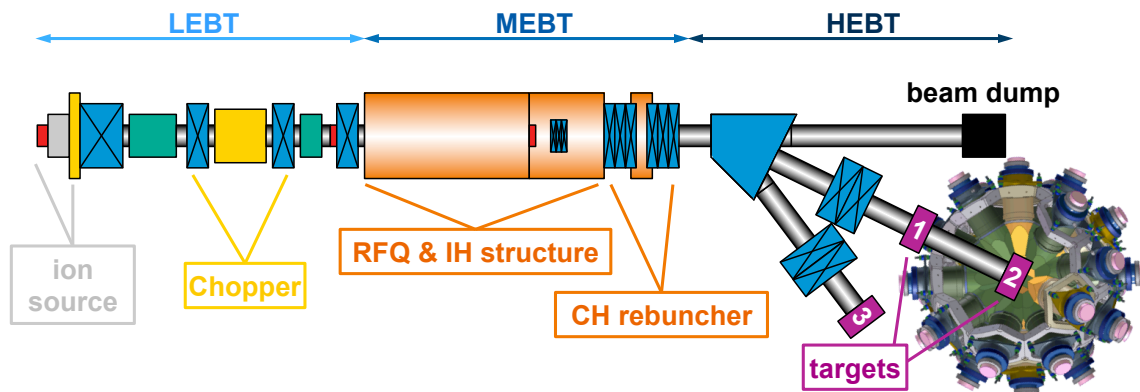


**Figure 3:** Schematic layout of the FRANZ facility, Frankfurt a.M., Germany. For details, see text.

This Medium-Energy Beam-Transport (MEFT) section is completed by a cross-bar H-mode (CH) rebuncher which allows the variation of the beam energy by 10%, therefore, energies from 1.8 MeV to 2.2 MeV are provided for the High-Energy Beam-Transport (HEBT) section serving the experimental setups [19]. The dipole magnet of the HEBT allows the deflection in three different beam-lines. The beam-dump is located straightforward while two experimental setups are available at deflection angles of  $40^\circ$  and  $80^\circ$ , respectively.

The beam-line at  $80^\circ$  is dedicated to experiments using the activation technique with neutrons as projectiles. The beam-line at  $40^\circ$  is optimized for in-beam experiments using a  $4\pi$   $\text{BaF}_2$  calorimeter [20] for the detection of prompt photons emitted in a radiative proton- or neutron-capture reaction, respectively.

A doublet of quadrupole magnets focuses the beam on either the neutron production target or the target for proton-capture. Figure 4 shows the results of the beam-transport simulation through the HEBT section using the simulation software TraceWin [21]. The envelope of the beam in  $x$  and  $y$  direction, *i.e.*, the  $3\sigma$  range where 99.7% of the beam intensity is located, is depicted with magnet settings optimized for target position 2 in Fig. 3. At distance 0 cm, the beam is delivered by the CH rebuncher with a diameter of 17 mm and 12 mm in  $x$  and  $y$  direction, respectively. The dipole magnet deflecting the beam into the  $40^\circ$  beam line is located at a distance of 38.3 cm. It focusses the beam in  $x$  direction, *i.e.*, in the deflection plane. Neglecting fringe fields, its influence in the  $y$  direction is negligible, thus, the high space charge of the beam yields defocussing.

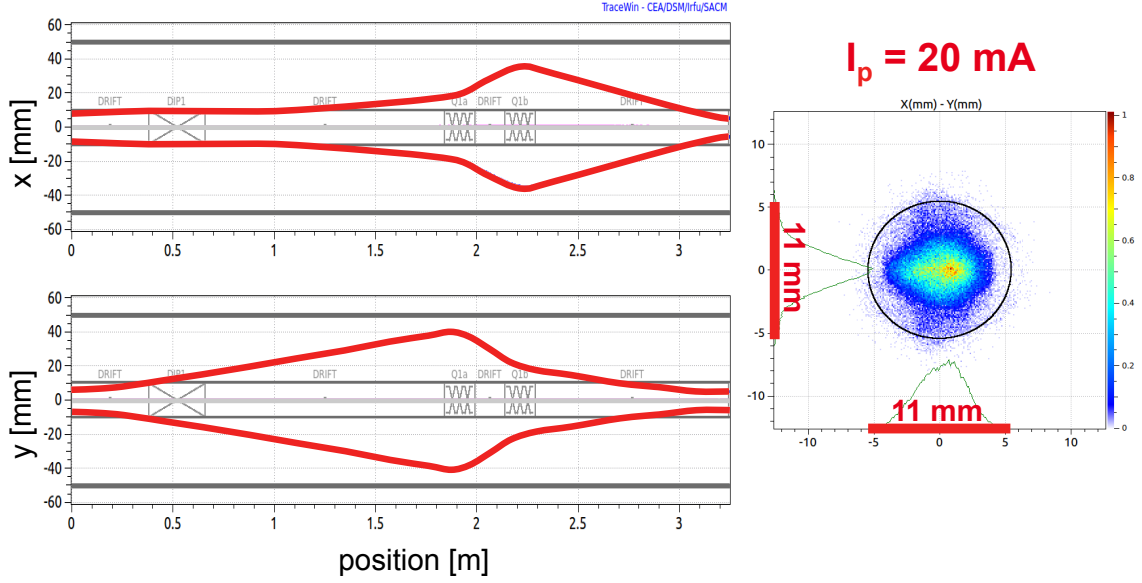


**Figure 4:** Simulation of beam transport in HEBT section of FRANZ. The left panels show the change of the envelope of the beam as a function of its position in the HEBT section. The right panel depicts the dimension of the beam at target position 2 in Fig. 3. For details, see text.

The quadrupole doublet at a distance of 184 cm focuses first in  $x$  and then in  $y$  direction. It is possible to confine the beam diameter at target position (325 cm distance) to values of  $\Delta x = 11$  mm and  $\Delta y = 11$  mm. Compared to beams with lower intensities as delivered from, *e.g.*, tandem accelerators, the resulting beam spot is quite large. However, the high intensity and the resulting high power deposition require a broad area where the beam hits the target to avoid damage of the target. In our case, the areal power density is about  $105$  W/cm<sup>2</sup>.

Therefore, cooling by a high-pressure water-flow might still be sufficient if an optimized combination of target and backing material is found. When investigating the  $^{91}\text{Nb}(p,\gamma)$  reaction using calorimetry of the prompt  $\gamma$  rays, as foreseen at FRANZ, the  $Q$  values of all reactions occurring in the backing material should be much lower than  $Q(^{91}\text{Nb}_{(p,\gamma)}) = 7458$  keV. Given the need of a high thermal conductivity to ensure a sufficient heat transfer from the target to the water, the most suitable material is tungsten. The highest  $Q$  value of its isotopes is  $Q(^{186}\text{W}_{(p,\gamma)}) = 5997$  keV and its thermal conductivity amounts to  $k = 174.0$  W m<sup>-1</sup>K<sup>-1</sup>.

Extensive simulations using the characteristics of the beam as discussed above showed that the

temperature will not exceed 200°C if the current is limited to  $E_p = 2$  mA. Thus, neither the target material nor any of the material used for mounting will be damaged. An experimental verification using a prototype as shown in Fig. 5 are to be performed.

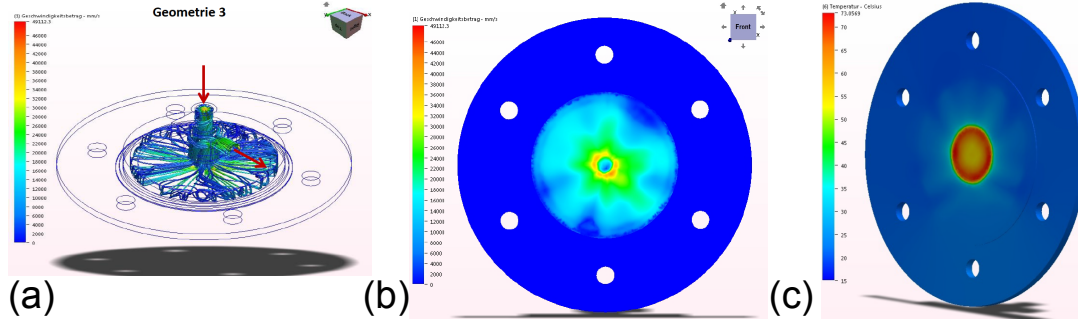


**Figure 5:** Exemplary simulation of high-pressure water-flow cooling. (a) Geometry of the inlet and outlet apertures. (b) Velocity distribution of water-flow projected on backing material. (c) Temperature distribution in the backing material. Taken from [22].

#### 4. Summary

The high-intensity low-energy proton-beam provided by the FRANZ facility, Frankfurt a.M., Germany, can be used to investigate radiative proton-capture reactions on unstable isotopes in standard kinematics. The construction of the HEBT [19], developments concerning an effective cooling mechanism for the targets [22], an adapted target chamber [23], and a high-rate detection system [24] are currently ongoing. First results are expected soon.

#### References

- [1] D. L. Lambert, *Astron. Astroph. Rev.* **3** (1992) 201.
- [2] M. Arnould, S. Goriely, *Phys. Rep.* **384** (2003) 1.
- [3] S. E. Woosley, W. M. Howard, *Astrophys. J. Suppl. Ser.* **36** (1978) 285.
- [4] H. Schatz, A. Aprahamian, J. Görres, M. Wiescher, T. Rauscher, J. Rembges, F.-K. Thielemann, B. Pfeiffer, P. Möller, K.-L. Kratz, H. Herndl, B. Brown, H. Rebel, *Phys. Rep.* **294** (1998) 167.
- [5] S. Goriely, J. José, M. Hernanz, M. Rayet, M. Arnould, *Astron. Astroph.* **383** (2002) L27.
- [6] C. Fröhlich, G. Martínez-Pinedo, M. Liebendörfer, F.-K. Thielemann, E. Bravo, W. R. Hix, K. Langanke, N. T. Zinner, *Phys. Rev. Lett.* **96** (2006) 142502.
- [7] S. E. Woosley, D. H. Hartmann, R. D. Hoffman, W. C. Haxton, *Astrophys. J.* **356** (1990) 272.
- [8] M. Kusakabe, N. Iwamoto, K. Nomoto, *Astrophys. J.* **726** (2011) 25.
- [9] C. Travaglio, F. Röpke, R. Gallino, W. Hillebrandt, *Astrophys. J.* **739** (2011) 93.
- [10] Gy. Gyürky, M. Vakulenko, Zs. Fülöp, Z. Halász, G. G. Kiss, E. Somorjai, T. Szücs, *Nucl. Phys.* **A922** (2014) 112.

- [11] A. Spyrou, S. J. Quinn, A. Simon, T. Rauscher, A. Battaglia, A. Best, B. Bucher, M. Couder, P. A. DeYoung, A. C. Dombos, X. Fang, J. Görres, A. Kontos, Q. Li, L. Y. Lin, A. Long, S. Lyons, B. S. Meyer, A. Roberts, D. Robertson, K. Smith, M. K. Smith, E. Stech, B. Stefanek, W. P. Tan, X. D. Tang, M. Wiescher, *Phys. Rev. C* **88** (2013) 045802.
- [12] N. A. Roughton, M. R. Fritts, R. J. Peterson, C. S. Zaidins, C. J. Hansen, *At. Data Nucl. Data Tables* **23** (1979) 177.
- [13] C. E. Laird, D. Flynn, R. L. Hershberger, F. Gabbard, *Phys. Rev. C* **35** (1987) 1265.
- [14] L. Netterdon, V. Derya, J. Endres, C. Fransen, A. Hennig, J. Mayer, C. Müller-Gatermann, A. Sauerwein, P. Scholz, M. Spieker, A. Zilges, *Nucl. Instr. and Meth. Phys. Res. A* **754** (2014) 94 .
- [15] A. Sauerwein, J. Endres, L. Netterdon, A. Zilges, V. Foteinou, G. Provasas, T. Konstantinopoulos, M. Axiotis, S. F. Ashley, S. Harissopulos, T. Rauscher, *Phys. Rev. C* **86** (2012) 035802.
- [16] C. M. Baglin, *Nuclear Data Sheets* **114** (2013) 1293, online version (<http://www.nndc.bnl.gov>, July 23, 2014).
- [17] P. Erbacher, *Untersuchung der Reaktion  $^{90}\text{Zr}(p,\gamma)$  mit In-Beam-Gammaspektroskopie*, Master Thesis, Goethe Universität Frankfurt a.M., unpublished, 2014.
- [18] R. Reifarh, C. Lederer, F. Käppeler, *J. Phys. G* **41** (2014) 053101.
- [19] O. Hinrichs, *Design und Aufbau der Hochenergie-Strahltransportführung an FRANZ*, PhD Thesis, Goethe Universität Frankfurt a.M., in progress.
- [20] K. Wisshak, K. Guber, F. Käppeler, J. Krisch, H. Müller, G. Rupp, F. Voss, *Nucl. Instr. Meth. A* **292** (1990) 595.
- [21] D. Uriot, TraceWin, online description (<http://irfu.cea.fr/Sacm/logiciels/index3.php>, July 29, 2014).
- [22] M. Reich, *Auswahl von Backing-Materialien für hochleistungsbeständige Proben an FRANZ*, Bachelor Thesis, Goethe Universität Frankfurt a.M., unpublished, 2013.
- [23] C. Arda, *Entwurf einer Targetkammer zum Einsatz in  $(p,\gamma)$ -Experimenten an FRANZ*, Bachelor Thesis, Goethe Universität Frankfurt a.M., unpublished, 2014.
- [24] C. Wolf, *Charakterisierung des 42-fach segmentierten  $4\pi$  BaF<sub>2</sub>-Detektors für FRANZ*, Bachelor Thesis, Goethe Universität Frankfurt a.M., unpublished, 2013.